

Sequential Dihydrogen Desorption from Hydride-Protected Atomically Precise Silver Clusters and the Formation of Naked Clusters in the Gas Phase

Atanu Ghosh, Mohammad Boduzzaman, Abhijit Nag, Madhuri Jash, Ananya Baksi,[†] and Thalappil Pradeep*^{ID}

Department of Chemistry, DST Unit of Nanoscience (DST UNS) and Thematic Unit of Excellence (TUE), Indian Institute of Technology Madras, Chennai 600 036, India

Supporting Information

ABSTRACT: We report the formation of naked cluster ions of silver of specific nuclearities, uncontaminated by other cluster ions, derived from monolayer-protected clusters. The hydride and phosphine co-protected cluster, $[Ag_{18}(TPP)_{10}H_{16}]^{2+}$ (TPP, triphenylphosphine), upon activation produces the naked cluster ion, Ag_{17}^+ , exclusively. The number of metal atoms present in the naked cluster is almost the same as that in the parent material. Two more naked cluster ions, Ag_{21}^+ and Ag_{19}^+ , were also formed starting from two other protected clusters, $[Ag_{25}(DPPE)_8H_{22}]^{3+}$ and $[Ag_{22}(DPPE)_8H_{19}]^{3+}$, respectively

(DPPE, 1,2-bis(diphenylphosphino)ethane). By systematic fragmentation, naked clusters of varying nuclei are produced from Ag_{17}^+ to Ag_1^+ selectively, with systematic absence of Ag_{10}^+ , Ag_6^+ , and Ag_4^+ . A seemingly odd number of cluster ions are preferred due to the stability of the closed electronic shells. Sequential desorption of dihydrogen occurs from the cluster ion, $Ag_{17}H_{14}^+$, during the formation of Ag_n^+ . A comparison of the pathways in the formation of similar naked cluster ions starting from two differently ligated clusters has been presented. This approach developed bridges the usually distinct fields of gas-phase metal cluster chemistry and solution-phase metal cluster chemistry. We hope that our findings will enrich nanoscience and nanotechnology beyond the field of clusters.

KEYWORDS: monolayer-protected clusters, naked clusters, gas-phase clusters, $Ag_{17}H_{14}^+$, Ag_{17}^+ , dihydrogen, mass spectrometry, nanomaterials



Naked clusters of metals produced by laser desorption, sputtering, and thermal evaporation have been studied intensely in the past several years.^{1–7} Unusual chemical reactivity, origin of catalysis, emergence of metallicity, etc., are some of the fascinating aspects of the science of these systems, prompting interdisciplinary studies.^{1,8–11} The feasibility to create monolayer-protected atomically precise clusters of varying nuclearities suggests the possibility to generate naked clusters at will by ligand desorption. Although the synthesis of such naked clusters appears simple, ligand desorption can lead to significant changes in the core structure, especially when the core–ligand interaction is strong ($\Delta H_f = 418$ kJ/mol as in the case of gold clusters protected with thiolates).^{12–20} Consequently, the naked clusters observed are very small such as Ag_4^+ , Ag_5^+ , and Ag_7^+ from well-known clusters such as $Ag_{25}(pMBA)_{18}$ and $Ag_{36}(pMBA)_{24}$ (*pMBA* = *para*-mercaptopbenzoic acid).¹³ Formation of even such very small naked

cluster cores has not been observed for protected silver clusters.^{21–23} The recent synthesis of hydride-rich silver clusters, co-protected by phosphines in solution, suggests easy desorption of weakly interacting ligands and consequent formation of large naked silver cluster ions.²⁴ This paper reports the formation of naked cluster ions of specific nuclearities, uncontaminated by other cluster ions where the number of metal atoms present in the naked cluster is almost the same as that in the parent material. By systematic fragmentation, clusters of varying nuclearities are produced with ease, paving the way for systematic investigation of their chemistry. Pathways for the formation of such naked cluster ions have been explored.

Received: July 30, 2017

Accepted: October 17, 2017

Published: October 17, 2017



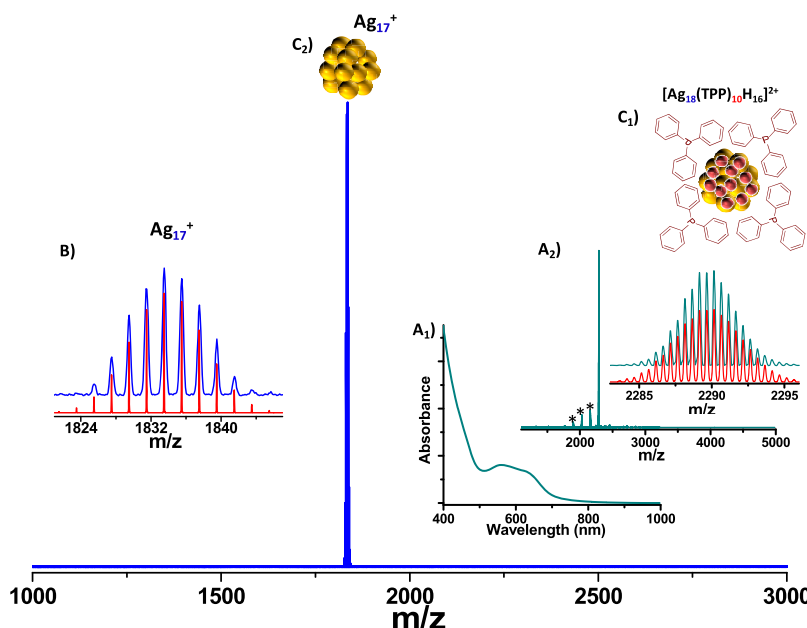


Figure 1. Mass spectrum of naked cluster ion (Ag_{17}^+) produced from cluster I. The absence of other peaks in the mass range of m/z 1000–3000 confirms that the product is uncontaminated by other cluster ions. Insets: (A₁) UV-vis spectrum of the parent cluster I in methanol; (A₂) full-range ESI MS spectrum of cluster I. The experimental (olive) and simulated (red trace) isotopic distributions are compared in the inset, which confirms the assigned composition of the parent cluster I, $[\text{Ag}_{18}(\text{TPP})_{10}\text{H}_{16}]^{2+}$. Peaks marked with black asterisks (*) are due to multiple phosphine losses from the parent cluster. (B) Simulated isotopic distribution (red trace) of Ag_{17}^+ ion is compared with the experimental data (blue trace). Exact matching of the two spectra confirms the assignment. Schematic illustrations of the protected parent cluster I (C₁) and the naked cluster (C₂). All phosphines are not shown in C₁.

Adsorption of hydrogen on transition metal surfaces is a popular area of research because of its application in heterogeneous catalysis and fuel cells.^{25–29} A number of reports are available in the literature on the understanding of associative desorption of dihydrogen from transition metal surfaces.³⁰ In many cases, hydrogen-adsorbed solid surfaces act as hydrogen sources.^{31–33} Effects of adsorbed hydrogen on the catalytic activity of transition metals have also been studied in detail.^{28,29} Here, we isolated a gaseous species, $\text{Ag}_{17}\text{H}_{14}^+$, which also undergoes associative desorption of seven hydrogen molecules (7H_2), leading to the formation of naked Ag_{17}^+ ion.

RESULTS AND DISCUSSION

We have used hydride-rich silver clusters reported by the Bakr group for our experiments. $[\text{Ag}_{18}(\text{TPP})_{10}\text{H}_{16}]^{2+}$ and $[\text{Ag}_{18}(\text{TPP})_{10}\text{D}_{16}]^{2+}$ (TPP, triphenylphosphine) were synthesized by modifying the procedure used for $\text{Ag}_{51}(\text{BDT})_{19}(\text{TPP})_3$ (BDT, 1,3-benzenedithiol).²⁴ Another two clusters, $[\text{Ag}_{25}(\text{DPPE})_8\text{H}_{22}]^{3+}$ and $[\text{Ag}_{22}(\text{DPPE})_8\text{H}_{19}]^{3+}$, were synthesized following the procedure reported by the Bakr group (DPPE, 1,2-bis(diphenylphosphino)ethane).²⁴ Hereafter, we will refer to $[\text{Ag}_{18}(\text{TPP})_{10}\text{H}_{16}]^{2+}$, $[\text{Ag}_{25}(\text{DPPE})_8\text{H}_{22}]^{3+}$, and $[\text{Ag}_{22}(\text{DPPE})_8\text{H}_{19}]^{3+}$ clusters as clusters I, II, and III, respectively. Details of the synthetic procedures are given in the Materials and Methods section. Structures of these clusters have not been solved yet.²⁴ After being cleaned, the synthesized clusters were dissolved in methanol and used for experiments. The UV-vis and mass spectra of cluster I are shown in Figure 1A₁, A₂, respectively. Comparison of the experimental and simulated isotopic distributions confirms the assigned composition (inset of Figure 1A₂). UV-vis and mass spectra of clusters II and III are shown in Figure S1, which match well with the reported data. After complete characterization, the

clusters were used for the synthesis of naked cluster ions in the gas phase.

Atomically precise, uncontaminated naked cluster ion Ag_{17}^+ was produced from cluster I using mass spectrometry. Electrospray ionization mass spectrometry (ESI MS) was performed using a Waters Synapt G2-Si high-definition mass spectrometer equipped with electrospray ionization, matrix-assisted laser desorption ionization, and ion mobility separation. Mass spectrum of the naked Ag_{17}^+ cluster ion is shown in Figure 1. The peak at m/z 1833.1 corresponds to Ag_{17}^+ . The isotopic structures of silver are quite useful to assign the exact composition. Silver has ^{107}Ag and ^{109}Ag isotopes with nearly similar abundances. The isotopic distribution is likely to reflect on the characteristic features of this cluster. The experimental (blue trace) and simulated (red trace) isotopic distributions are compared in Figure 1B. Exact match of the two spectra confirms the assignment. ESI MS data (Figure 1) show that the cluster ions formed are in highly pure state as no peaks other than Ag_{17}^+ are found in the mass range of m/z 1000–3000. The naked Ag_{17}^+ cluster ion is generated by applying higher cone voltage (150 V). Details of the instrument and conditions are given in the Materials and Methods section and Supporting Information. The process of naked cluster formation does not involve any mass selection. Cone voltage-dependent total ligand desorption from cluster I is described in a later section of the article. We have also demonstrated the creation of two more naked cluster ions, Ag_{21}^+ and Ag_{19}^+ , from clusters II and III, respectively, using mass spectrometry/mass spectrometry (MS/MS) (Figure S2). Here, the intensities of the naked cluster ions are quite less than that of the Ag_{17}^+ ion as the process involves mass selection.

The formation of a hydrogen-free naked Ag_{17}^+ cluster ion was further confirmed by using the deuterated parent material, $[\text{Ag}_{18}(\text{TPP})_{10}\text{D}_{16}]^{2+}$. There is a shift in the peak position of

parent cluster I when hydrogen atoms are replaced with the deuterium atoms (Figure 2A). Black and red traces correspond

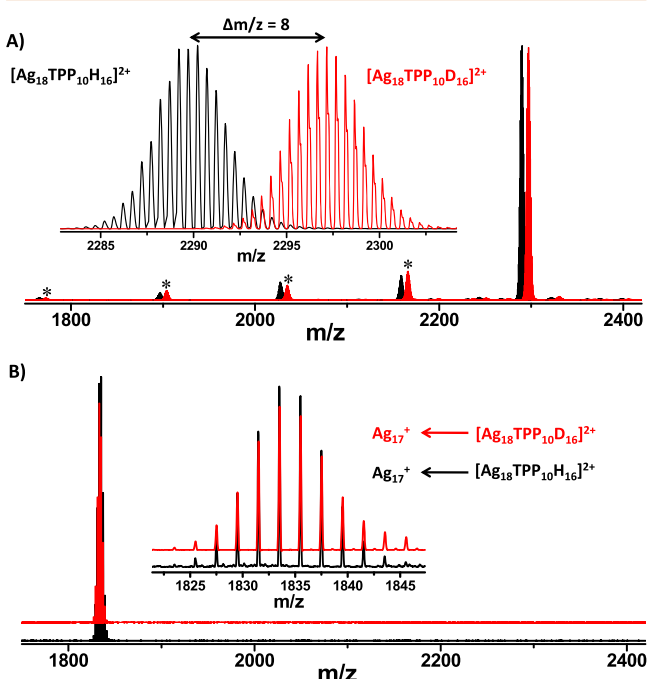


Figure 2. (A) ESI MS spectra of the parent materials $[Ag_{18}(TPP)_{10}H_{16}]^{2+}$ (black trace) and $[Ag_{18}(TPP)_{10}D_{16}]^{2+}$ (red trace). Peaks with asterisks (*) are due to $[Ag_{18}(TPP)_{10-n}D_{16}]^{2+}$ (where $n = 1, 2, 3, 4, \dots$). Inset: Corresponding peaks are expanded. (B) Naked Ag_{17}^+ cluster ions produced from the H (black trace) and D (red trace) protected parent clusters, respectively. Inset: Corresponding peaks are expanded. Exact match in the isotopic distributions confirms the absence of hydrogen atoms of the naked Ag_{17}^+ cluster ion.

to the parent clusters, $[Ag_{18}(TPP)_{10}H_{16}]^{2+}$ and $[Ag_{18}(TPP)_{10}D_{16}]^{2+}$, respectively. Inset of Figure 2A shows that the peak is shifted by $\Delta m/z = 8$, due to the replacement of 16 hydrogen atoms (m/z 16) by deuterium atoms (m/z 32). The naked cluster ions produced from both materials appear at the same position, as expected (m/z 1833.1, Figure 2B). The peaks are expanded in the inset of Figure 2B, which shows an exact match in the isotopic distributions. It confirms the absence of hydrogen atoms in the naked Ag_{17}^+ cluster ion.

Next, we attempted to produce all the lower naked silver ions starting from Ag_{17}^+ . Systematic fragmentation of Ag_{17}^+ ion was performed using the MS/MS technique. The collision energy (CE)-dependent fragmentations of Ag_{17}^+ are presented in Figure 3. Details of the other instrumental conditions for the MS/MS study are given in the experimental section of the Supporting Information. Fragmentation of Ag_{17}^+ ion starts at CE 5 (black trace). The intensity of the peak corresponding to Ag_{17}^+ ion decreases with increasing CE, resulting in the formation of clusters of lower masses. At higher CE, the peak corresponding to Ag_{17}^+ ion has disappeared completely (blue trace). Finally, the peak corresponding to naked Ag_1^+ ion was observed at CE 200 (violet trace). Almost all the ions starting from Ag_1^+ to Ag_{17}^+ were formed. Surprisingly, Ag_4^+ , Ag_6^+ , and Ag_{10}^+ ions were not seen during such fragmentation. The expected peak positions corresponding to these ions are marked with dotted red lines in Figure 3. For more clarity, the Ag_4^+ , Ag_6^+ , and Ag_{10}^+ regions are expanded in Figures S3

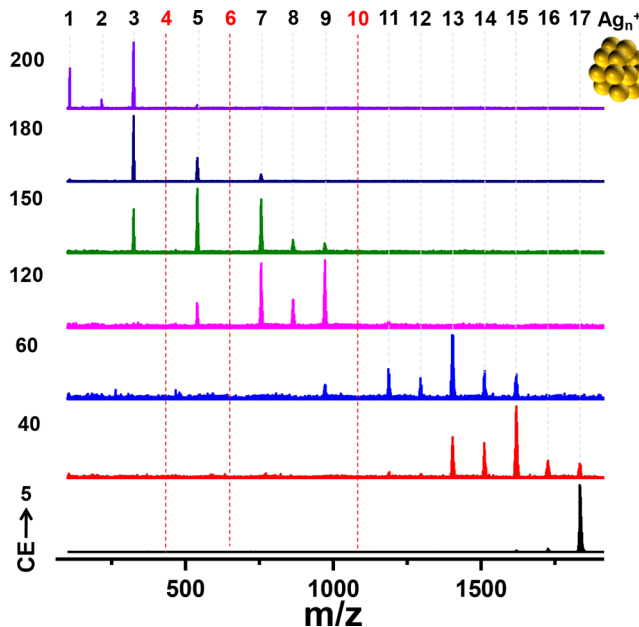


Figure 3. Collision energy (CE)-dependent MS/MS spectra of the Ag_{17}^+ ion. Almost all the ions (Ag_n^+) starting from Ag_{17}^+ to Ag_1^+ are formed except Ag_{10}^+ , Ag_6^+ , and Ag_4^+ . Absence of these ions is marked with red dotted lines. CEs (in instrumental units) are marked.

and S4. The absence of Ag_4^+ and Ag_{10}^+ ions can be explained with the superatom model, according to which systems with 2, 8, 18... electrons have better stability in the gas phase. Ag_3^+ and Ag_9^+ ions have higher stability as they contain 2 and 8 electrons, respectively.^{34–36} Because of this reason, Ag_5^+ ion is directly fragmented to Ag_3^+ ion during the MS/MS process and not via Ag_4^+ (a three-electron system). The same is true for the direct conversion of Ag_{11}^+ to Ag_9^+ ion, which does not involve any Ag_{10}^+ (a nine-electron system).

During production of the naked cluster ion, Ag_{17}^+ , from the protected cluster I, a species protected only with hydrogen was observed. The assignment of the species, $Ag_{17}H_{14}^+$, was confirmed from a comparison of the experimental and simulated isotopic distributions (Figure S5). The presence of 14 hydrogen atoms is further confirmed by synthesizing the deuterium analogue of $Ag_{17}H_{14}^+$ (*i.e.*, $Ag_{17}D_{14}^+$). The spectra are shown in Figure S6. Mass difference $\Delta m/z = 14$ confirms the assignment, $Ag_{17}H_{14}^+$. Formation of $Ag_{17}H_{14}^+$ ion from the parent cluster I is described in a later section of the article.

We were curious to know how the hydrogen atoms were knocked out from $Ag_{17}H_{14}^+$ during the formation of Ag_{17}^+ ion. To study this, cone voltage-dependent conversion of $Ag_{17}H_{14}^+$ to Ag_{17}^+ cluster was investigated (Figure 4A). One of the experimental spectra shown in Figure 4A (red trace) are compared with the simulated spectra. The comparisons are shown in Figure 4B. The positions of the simulated spectra of Ag_{17}^+ ions with the even number of hydrogen atoms (blue traces) are matching exactly with the experimental data (red trace), whereas the spectra of an odd number of hydrogen atoms (olive traces) do not show such type of matching. It confirms the existence of an even number of hydrogen-protected Ag_{17}^+ cluster ions during the conversion process. The above observation suggests that the hydrogen atoms are knocked out from the $Ag_{17}H_{14}^+$ cluster ion as dihydrogen (H_2). Sequential loss of dihydrogen from the surface of an

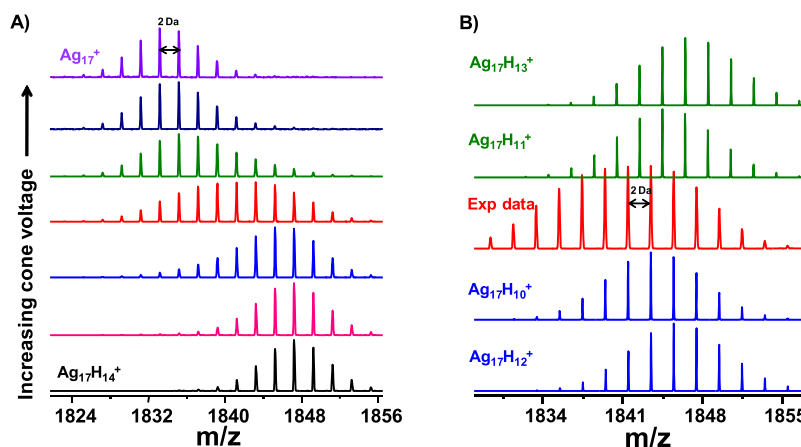


Figure 4. (A) Cone voltage-dependent conversion of $\text{Ag}_{17}\text{H}_{14}^+$ to Ag_{17}^+ cluster ion. The peak separation in Ag_{17}^+ is due to the silver isotopes. (B) Mass spectrum of one of the intermediates (red trace in A) of the conversion process of $\text{Ag}_{17}\text{H}_{14}^+$ to Ag_{17}^+ is compared with the simulated spectra of $\text{Ag}_{17}\text{H}_n^+$. For $n = \text{even}$, positions of the simulated spectra (blue traces) match the experimental spectra (red traces). Such type of matching is not observed when $n = \text{odd}$ (olive traces). Dihydrogen loss and the isotope distribution of silver lead to the spacing of 2 Da in the experimental data.

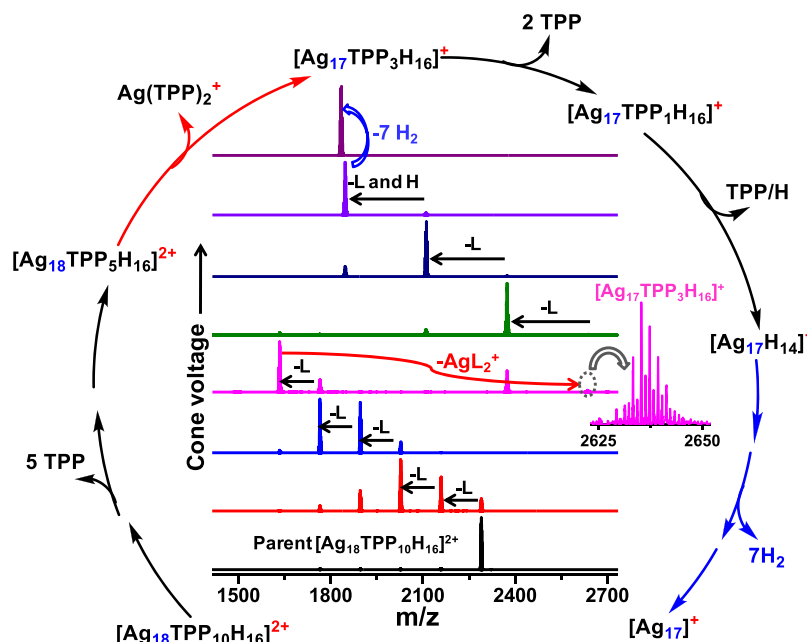


Figure 5. Pathway for the formation of naked cluster ion Ag_{17}^+ from the protected cluster I. Inset: Cone voltage-dependent mass spectra. The peak corresponding to $[\text{Ag}_{17}(\text{TPP})_3\text{H}_{16}]^+$ ion is expanded (pink trace). TPP is represented by "L". The peak corresponding to Ag_{17}^+ ion is observed at a cone voltage of 150 V. Changes in the charge state and the dihydrogen desorption steps are marked with red and blue arrows, respectively. The process does not involve any mass selection.

atomically precise cluster (gaseous $\text{Ag}_{17}\text{H}_{14}^+$) has not been observed before.

We have created naked cluster ions from the protected cluster where the number metal atoms are almost the same as the parent material. Change in the charge state was also observed from the parent (+2) to the naked cluster (+1). So it was quite important to explore the fragmentation pathways of such a process. The cone voltage-dependent fragmentation pathway of cluster I is shown in Figure 5. Corresponding mass spectra are shown in the inset of Figure 5. Initially, the parent ion $[\text{Ag}_{18}(\text{TPP})_{10}\text{H}_{16}]^{2+}$ (m/z 2290.0) undergoes sequential loss of five TPP ligands to produce $[\text{Ag}_{18}(\text{TPP})_5\text{H}_{16}]^{2+}$ (m/z 1634.3). By losing one $[\text{Ag}(\text{TPP})_2]^+$ unit, doubly charged $[\text{Ag}_{18}(\text{TPP})_5\text{H}_{16}]^{2+}$ is converted to singly charged $[\text{Ag}_{17}(\text{TPP})_3\text{H}_{16}]^+$ (m/z 2635.5). The peak corresponding to

this singly charged species is expanded in the inset of Figure 5 (pink trace). The charge-stripping step is marked with a red arrow in Figure 5. It further loses two TPP ligands followed by the loss of one TPP ligand and hydrogens to produce $\text{Ag}_{17}\text{H}_{14}^+$ (m/z 1847.1). Sequential loss of seven dihydrogen molecules (H_2) from the $\text{Ag}_{17}\text{H}_{14}^+$ species leads to the formation of the naked Ag_{17}^+ (m/z 1833.1) ion. The hydrogen desorption steps are marked with blue arrows in Figure 5. Steps involved in the formation of the Ag_{17}^+ ion from the $\text{Ag}_{17}\text{H}_{14}^+$ species are shown in Figure 4A. Simulated peak positions are compared with the experimental data (Table S1 in Supporting Information), which confirm all the above assignments. Unlike cluster I, clusters II and III do not produce naked cluster ions at higher cone voltages.

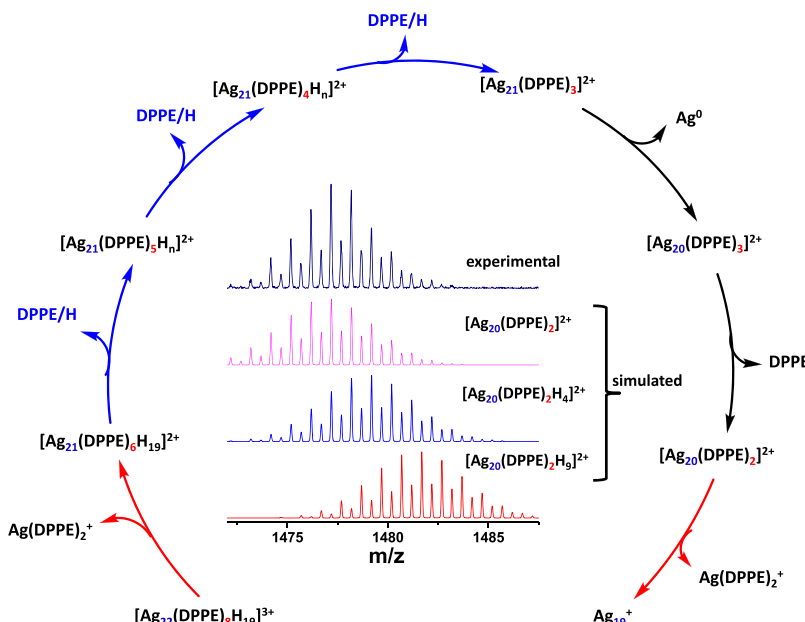


Figure 6. Different species formed during the fragmentation of cluster III (*i.e.*, the formation of Ag_{19}^+). Change in the charge state and the hydrogen desorption steps are marked with red and blue arrows, respectively. The process involves mass selection. Inset: Comparison of experimental spectrum (deep blue trace, topmost) with the simulated spectra (red, blue, and pink traces), which confirms the formation of $[\text{Ag}_{20}(\text{DPPE})_2]^{2+}$.

Formation of naked clusters were also investigated by tandem mass spectrometry. Clusters II and III produce naked cluster ions Ag_{21}^+ and Ag_{19}^+ , respectively, during MS/MS study (Figure S2). Such observations drive us to compare the fragmentation pathways of clusters I, II, and III. Collision energy-dependent fragmentation pathway of cluster I follows the same pathway as shown in the Figure 5. Cluster I loses all of the TPP ligands initially and produces $\text{Ag}_{17}\text{H}_{14}^+$, which further loses hydrogen to generate the naked cluster ion. Unlike cluster I, cluster III starts to lose DPPE ligands and hydrogens simultaneously (Figure 6). Initially, the 3+ charge state of the parent cluster III converts to 2+ by losing one $[\text{Ag}(\text{DPPE})_2]^+$ unit. The charge-stripping step is marked with a red arrow. At higher collision energy, cluster III loses all the hydrogens and a few DPPE ligands, resulting in the formation of $[\text{Ag}_{20}(\text{DPPE})_2]^{2+}$ (m/z 1477.2), which further loses one $[\text{Ag}(\text{DPPE})_2]^+$ unit to produce the naked Ag_{19}^+ ion. Mass spectra corresponding to different steps involved in the formation of Ag_{19}^+ ion from cluster III are shown in Figure S7. The peaks are expanded in Figure S8. Mass of a DPPE ligand is 398.42. So mass loss of m/z 199 is equivalent to one DPPE ligand as the charge state is 2+. Green arrow represents the loss of maximum hydrogens (Figure S8). Loss of 16 hydrogens was observed at this step (Figure S8). The formation of the $[\text{Ag}_{20}(\text{DPPE})_2]^{2+}$ ion is confirmed by comparing the experimental and calculated data (inset of Figure 6). It also confirms the complete loss of all the hydrogen atoms from cluster III. We further confirmed the formation of hydrogen-free $[\text{Ag}_{20}(\text{DPPE})_2]^{2+}$ ion by comparing the fragmentation data of the deuterated analogue of cluster III. Mass spectra of parent cluster III and its deuterated analogues are shown in Figure S9A. Mass spectra of $[\text{Ag}_{20}(\text{DPPE})_2]^{2+}$ ions generated from the H (black trace) and D (red trace) protected parent clusters are compared in Figure S9B. Exact match of the peak positions confirms the complete removal of H or D and the formation of $[\text{Ag}_{20}(\text{DPPE})_2]^{2+}$ ion. DPPE-protected cluster II also follows

the same fragmentation pathway like cluster III. Here, we confirmed the complete removal of hydrogens and formation of $[\text{Ag}_{24}(\text{DPPE})_2]^{2+}$ ion by comparing its mass spectrum with that derived from the deuterated analogues (Figure S10). Positions of the naked cluster ions, Ag_{19}^+ and Ag_{21}^+ (generated from deuterated analogues, Figure S11), match exactly with those shown in Figure S2. Such fragmentation pathways suggest that the DPPE ligands are more strongly bonded with the metal core than the TPP ligands. We believe that in cluster I, TPP ligands are connected with the metal core through one phosphine end, whereas DPPE ligands use two phosphine ends in cluster III. DPPE-protected cluster II also follows the same fragmentation pathway like cluster III. The above observation implies that the number of phosphine ends of a ligand connected with the metal core plays an important role in the formation of naked cluster ions without involving mass selection.

CONCLUSION

In conclusion, atomically pure naked cluster ions Ag_{17}^+ , Ag_{19}^+ , and Ag_{21}^+ were created from the ligand-protected clusters, $[\text{Ag}_{18}(\text{TPP})_{10}\text{H}_{16}]^{2+}$, $[\text{Ag}_{22}(\text{DPPE})_8\text{H}_{19}]^{3+}$, and $[\text{Ag}_{25}(\text{DPPE})_8\text{H}_{22}]^{3+}$, respectively. Notably, the number of metal atoms present in the naked cluster is almost the same as that in the parent material. We explored the different steps involved in the formation of the naked cluster ions from two differently ligated (TPP and DPPE) clusters. As such clusters (Ag_{17}^+) can be created at ambient conditions, without mass selection, their deposition can create cluster-assembled solids. Because clusters are produced from solutions during electrospray, it is possible to pattern the structures derived from the spray, and with clusters of different nuclearities now accessible, these cluster-assembled solids may be possible with an array of cluster systems. Such naked clusters could open the door to an exciting field of study of cluster reactions in the gas phase, starting with solution-phase clusters that can be synthesized in

very large quantities. During the fragmentation of $[Ag_{18}(TPP)_{10}H_{16}]^{2+}$, we have isolated a species, $Ag_{17}H_{14}^+$. Sequential loss of seven dihydrogen molecules ($7H_2$) was observed from $Ag_{17}H_{14}^+$ cluster ion in the gas phase. Associative desorption of hydrogen from metal cluster ions in the gas phase will be an interesting aspect of research in the future. Such isolated gaseous $Ag_{17}H_{14}^+$ species can be used as a potential source of hydrogen molecules for diverse applications. The naked metal cluster ions may be used for applications in catalysis, patterning, spectroscopy, etc., expanding the scope of cluster science.

Composition of such clusters is tunable, and there is a possibility to create naked alloy clusters by the same approach. All of these together can expand the scope of cluster science to catalysis, photonic materials, plasmonic crystals, porous materials, and other areas. Soluble ligand-protected clusters with weakly binding ligands is one of the major reasons for the success of this experiment. Need for naked clusters with precise nuclearity would intensify the search for better ligands that can leave without affecting the cluster core. It is likely that larger cluster alloys and more complex cluster systems may be made if easily leaving ligands are available. Naked clusters could become starting materials especially for gas-phase reactions. All of these will enhance the scope of cluster science. Although many of these are speculative right now, indications of research directions in the area of nanoparticles, quantum dots, and such materials suggest possibilities.

MATERIALS AND METHODS

Chemicals. Sodium borohydride ($NaBH_4$, 98%) and sodium borodeuteride ($NaBD_4$, 98 atom % D) were purchased from Sigma-Aldrich. Silver nitrate ($AgNO_3$) was purchased from Rankem Chemicals. Triphenylphosphine (TPP) and 1,2-bis(diphenylphosphino)ethane (DPPE) were purchased from Spectro-Chem. All the chemicals were used as received without further purification. All solvents (dichloromethane (DCM), *n*-hexane, methanol (MeOH), and chloroform ($CHCl_3$)) were purchased from Rankem and were of analytical grade. Water used in the synthesis was Milli-Q grade with a resistivity of 18.2 $M\Omega\cdot cm$.

Synthesis of $[Ag_{18}(TPP)_{10}H_{16}]^{2+}$ (Cluster I). The material was synthesized by modifying the procedure used for $Ag_{51}(BDT)_{19}(TPP)_3$. Initially, 20 mg of $AgNO_3$ was dissolved in 5 mL of methanol. Triphenylphosphine (70 mg in 10 mL of chloroform) was added to the above solution under stirring conditions. After 20 min of reaction, 6 mg of $NaBH_4$ dissolved in 0.5 mL of ice-cold Millipore water was added to the above reaction mixture. On addition of aqueous $NaBH_4$ solution, the colorless solution immediately turned light yellow. The stirring was continued for 3 h. Final color of the reaction mixture was deep green, which confirmed the formation of cluster I. The solvent was removed from the reaction mixture by rotary evaporation. The cluster was then washed 3–4 times with Millipore water to remove the unreacted silver ions and $NaBH_4$. After being washed, the green colored precipitate was dissolved in methanol for characterization. Following the same procedure, $[Ag_{18}TPP_{10}D_{16}]^{2+}$ was synthesized by replacing $NaBH_4$ with $NaBD_4$.

Synthesis of $[Ag_{25}(DPPE)_8H_{22}]^{3+}$ and $[Ag_{22}(DPPE)_8H_{19}]^{3+}$ (Clusters II and III). These materials were synthesized by following the reported procedure. Initially, 20 mg of $AgNO_3$ was dissolved in 5 mL of methanol. Seven milliliters of DCM solution containing 75 mg of DPPE was added to the above solution under stirring conditions. After 20 min of stirring, aqueous solution (1 mL) of $NaBH_4$ (35 mg) was added to the above mixture. Immediately, the color of the reaction mixture turned light yellow from colorless. The reaction was continued for 60 min. Formation of the Ag_{25} and Ag_{22} clusters was confirmed by the appearance of orange color reaction mixture. Solvent was removed from the reaction mixture by rotary vacuum evaporation. The material was washed with 10 mL of Millipore water to remove the excess silver

precursor and reducing agent. The process was repeated 3–4 times for complete removal of water-soluble ingredients. The purified material was dissolved in methanol for further characterization and use.

Mass Spectrometric Measurements. A Waters Synapt G2-Si high-definition mass spectrometer was used for all the ESI MS measurements. The instrument is equipped with electrospray ionization, matrix-assisted laser desorption ionization, and ion mobility separation. All of the samples were analyzed in the positive mode of electrospray ionization. The instrument calibration was done using CsI as the calibrant. Different instrumental conditions were used for the different types of measurements, as shown in the experimental section of the Supporting Information.

ASSOCIATED CONTENT

Supporting Information

The Supporting Information is available free of charge on the ACS Publications website at DOI: [10.1021/acsnano.7b05406](https://doi.org/10.1021/acsnano.7b05406).

Instrumental conditions for different types of measurements, additional experimental methods, additional ESI MS and UV/vis data ([PDF](#))

AUTHOR INFORMATION

Corresponding Author

*E-mail: pradeep@iitm.ac.in.

ORCID

Thalappil Pradeep: [0000-0003-3174-534X](https://orcid.org/0000-0003-3174-534X)

Author Contributions

A.G. designed and carried out the reactions. A.N. and A.B. carried out mass spectrometric measurements. T.P. supervised the whole project. The manuscript was written through contributions of all authors.

Notes

The authors declare no competing financial interest.

[†]Currently a postdoctoral fellow at Karlsruhe Institute of Technology, Germany.

ACKNOWLEDGMENTS

We thank the Department of Science and Technology for supporting our research program. A.G., Md.B., and M.J. thank UGC for their research fellowships. A.N. thanks IIT Madras for a research fellowship.

REFERENCES

- (1) Luo, Z.; Castleman, A. W.; Khanna, S. N. Reactivity of Metal Clusters. *Chem. Rev.* **2016**, *116*, 14456–14492.
- (2) Milani, P.; DeHeer, W. A. Improved Pulsed Laser Vaporization Source for Production of Intense Beams of Neutral and Ionized Clusters. *Rev. Sci. Instrum.* **1990**, *61*, 1835–8.
- (3) Wagner, R. L.; Vann, W. D.; Castleman, A. W., Jr. A Technique for Efficiently Generating Bimetallic Clusters. *Rev. Sci. Instrum.* **1997**, *68*, 3010–3013.
- (4) Bouwen, W.; Thoen, P.; Vanhoutte, F.; Bouckaert, S.; Despa, F.; Weidele, H.; Silverans, R. E.; Lievens, P. Production of Bimetallic Clusters by a Dual-Target Dual-Laser Vaporization Source. *Rev. Sci. Instrum.* **2000**, *71*, 54–58.
- (5) Keki, S.; Szilagyi, L. S.; Toeroek, J.; Deak, G.; Zsuga, M. High Aggregation Number Silver Clusters by Matrix-Assisted Laser Desorption/Ionization: Role of Matrixes on the Gas-Phase Reduction of Silver Ions. *J. Phys. Chem. B* **2003**, *107*, 4818–4825.
- (6) Baksi, A.; Pradeep, T.; Yoon, B.; Yannouleas, C.; Landman, U. Bare Clusters Derived from Protein Templates: Ag_{25}^+ , Ag_{38}^+ and Ag_{102}^+ . *ChemPhysChem* **2013**, *14*, 1272–1282.

- (7) Chakraborty, I.; Pradeep, T. Atomically Precise Clusters of Noble Metals: Emerging Link between Atoms and Nanoparticles. *Chem. Rev.* **2017**, *117*, 8208–8271.
- (8) Johnston, R. L. *Atomic and Molecular Clusters*; Taylor and Francis: London, 2002.
- (9) Luo, Z.; Gamboa, G. U.; Smith, J. C.; Reber, A. C.; Reveles, J. U.; Khanna, S. N.; Castleman, A. W., Jr. Spin Accommodation and Reactivity of Silver Clusters with Oxygen: The Enhanced Stability of Ag_{13} . *J. Am. Chem. Soc.* **2012**, *134*, 18973–18978.
- (10) Ervin, K. M. Metal-Ligand Interactions: Gas-Phase Transition Metal Cluster Carbonyls. *Int. Rev. Phys. Chem.* **2001**, *20*, 127–164.
- (11) Burgert, R.; Schnoeckel, H.; Grubisic, A.; Li, X.; Stokes, S. T.; Bowen, K. H.; Gantefoer, G. F.; Kiran, B.; Jena, P. Spin Conservation Accounts for Aluminum Cluster Anion Reactivity Pattern with O_2 . *Science (Washington, DC, U. S.)* **2008**, *319*, 438–442.
- (12) Jin, R.; Zeng, C.; Zhou, M.; Chen, Y. Atomically Precise Colloidal Metal Nanoclusters and Nanoparticles: Fundamentals and Opportunities. *Chem. Rev.* **2016**, *116*, 10346–10413.
- (13) Black, D. M.; Crittenden, C. M.; Brodbelt, J. S.; Whetten, R. L. Ultraviolet Photodissociation of Selected Gold Clusters: Ultraefficient Unstapling and Ligand Stripping of $\text{Au}_{25}(\text{pMBA})_{18}$ and $\text{Au}_{36}(\text{pMBA})_{24}$. *J. Phys. Chem. Lett.* **2017**, *8*, 1283–1289.
- (14) Angel, L. A.; Majors, L. T.; Dharmaratne, A. C.; Dass, A. Ion Mobility Mass Spectrometry of $\text{Au}_{25}(\text{SCH}_2\text{CH}_2\text{Ph})_{18}$ Nanoclusters. *ACS Nano* **2010**, *4*, 4691–4700.
- (15) Ghosh, A.; Udayabhaskararao, T.; Pradeep, T. One-Step Route to Luminescent $\text{Au}_{18}\text{SG}_{14}$ in the Condensed Phase and Its Closed Shell Molecular Ions in the Gas Phase. *J. Phys. Chem. Lett.* **2012**, *3*, 1997–2002.
- (16) Black, D. M.; Bhattachari, N.; Whetten, R. L.; Bach, S. B. H. Collision-Induced Dissociation of Monolayer Protected Clusters Au_{144} and Au_{130} in an Electrospray Time-of-Flight Mass Spectrometer. *J. Phys. Chem. A* **2014**, *118*, 10679–10687.
- (17) Fields-Zinna, C. A.; Sampson, J. S.; Crowe, M. C.; Tracy, J. B.; Parker, J. F.; deNey, A. M.; Muddiman, D. C.; Murray, R. W. Tandem Mass Spectrometry of Thiolate-Protected Au Nanoparticles $\text{Na}_x\text{Au}_{25}(\text{SC}_2\text{H}_4\text{Ph})_{18-y}(\text{S}(\text{C}_2\text{H}_4\text{O})_5\text{CH}_3)_y$. *J. Am. Chem. Soc.* **2009**, *131*, 13844–13851.
- (18) Dass, A.; Stevenson, A.; Dubay, G. R.; Tracy, J. B.; Murray, R. W. Nanoparticle MALDI-TOF Mass Spectrometry without Fragmentation: $\text{Au}_{25}(\text{SCH}_2\text{CH}_2\text{Ph})_{18}$ and Mixed Monolayer $\text{Au}_{25}(\text{SCH}_2\text{CH}_2\text{Ph})_{18-x}(\text{L})_x$. *J. Am. Chem. Soc.* **2008**, *130*, 5940–5946.
- (19) Dass, A.; Dubay, G. R.; Fields-Zinna, C. A.; Murray, R. W. FAB Mass Spectrometry of $\text{Au}_{25}(\text{SR})_{18}$ Nanoparticles. *Anal. Chem.* **2008**, *80*, 6845–6849.
- (20) Liu, C.; Lin, S.; Pei, Y.; Zeng, X. C. Semiring Chemistry of $\text{Au}_{25}(\text{SR})_{18}$: Fragmentation Pathway and Catalytic Active site. *J. Am. Chem. Soc.* **2013**, *135*, 18067–18079.
- (21) Chakraborty, P.; Baksi, A.; Khatun, E.; Nag, A.; Ghosh, A.; Pradeep, T. Dissociation of Gas Phase Ions of Atomically Precise Silver Clusters Reflects Their Solution Phase Stability. *J. Phys. Chem. C* **2017**, *121*, 10971–10981.
- (22) Wu, Z.; Lanni, E.; Chen, W.; Bier, M. E.; Ly, D.; Jin, R. High Yield, Large Scale Synthesis of Thiolate-Protected Ag_7 Clusters. *J. Am. Chem. Soc.* **2009**, *131*, 16672–16674.
- (23) Baksi, A.; Harvey, S. R.; Natarajan, G.; Wysocki, V. H.; Pradeep, T. Possible Isomers in Ligand Protected Ag_{11} Cluster Ions Identified by Ion Mobility Mass Spectrometry and Fragmented by Surface Induced Dissociation. *Chem. Commun. (Cambridge, U. K.)* **2016**, *52*, 3805–3808.
- (24) Bootharaju, M. S.; Dey, R.; Gevers, L. E.; Hedhili, M. N.; Bassett, J.-M.; Bakr, O. M. A New Class of Atomically Precise, Hydride-Rich Silver Nanoclusters Co-Protected by Phosphines. *J. Am. Chem. Soc.* **2016**, *138*, 13770–13773.
- (25) Oudenhuijzen, M. K.; van Bokhoven, J. A.; Miller, J. T.; Ramaker, D. E.; Koningsberger, D. C. Three-Site Model for Hydrogen Adsorption on Supported Platinum Particles: Influence of Support Ionicity and Particle Size on the Hydrogen Coverage. *J. Am. Chem. Soc.* **2005**, *127*, 1530–1540.
- (26) Oudenhuijzen, M. K.; van Bokhoven, J. A.; Miller, J. T.; Ramaker, D. E.; Koningsberger, D. C. Three-Site Model for Hydrogen Adsorption on Supported Platinum Particles: Influence of Support Ionicity and Particle Size on the Hydrogen Coverage. *J. Am. Chem. Soc.* **2005**, *127* (5), 1530–1540.
- (27) Bus, E.; van Bokhoven, J. A. Hydrogen Chemisorption on Supported Platinum, Gold, and Platinum-Gold-Alloy Catalysts. *Phys. Chem. Chem. Phys.* **2007**, *9*, 2894–2902.
- (28) Aleksandrov, H. A.; Kozlov, S. M.; Schauermann, S.; Vayssilov, G. N.; Neyman, K. M. How Absorbed Hydrogen Affects the Catalytic Activity of Transition Metals. *Angew. Chem., Int. Ed.* **2014**, *53*, 13371–13375.
- (29) Gudmundsdottir, S.; Skulason, E.; Weststrate, K.-J.; Juurlink, L.; Jonsson, H. Hydrogen Adsorption and Desorption at the Pt(110)-(1 × 2) Surface: Experimental and Theoretical Study. *Phys. Chem. Chem. Phys.* **2013**, *15*, 6323–6332.
- (30) Thuault-Cytermann, C.; Desjonquieres, M. C.; Spanjaard, D. Adsorption of Hydrogen on b.c.c. Transition-Metal Surfaces. *J. Phys. C: Solid State Phys.* **1983**, *16*, 5689.
- (31) Gudmundsdottir, S.; Skulason, E.; Jonsson, H. Reentrant Mechanism for Associative Desorption: $\text{H}_2/\text{Pt}(110)-(1 \times 2)$. *Phys. Rev. Lett.* **2012**, *108*, 156101.
- (32) Züttel, A. Materials for Hydrogen Storage. *Mater. Today* **2003**, *6*, 24–33.
- (33) Crawford, P.; Hu, P. The Importance of Hydrogen's Potential-Energy Surface and the Strength of the Forming R-H Bond in Surface Hydrogenation Reactions. *J. Chem. Phys.* **2006**, *124*, 044705.
- (34) Castleman, A. W.; Khanna, S. N. Clusters, Superatoms, and Building Blocks of New Materials. *J. Phys. Chem. C* **2009**, *113*, 2664–2675.
- (35) Reveles, J. U.; Khanna, S. N.; Roach, P. J.; Castleman, A. W. Multiple Valence Superatoms. *Proc. Natl. Acad. Sci. U. S. A.* **2006**, *103*, 18405–18410.
- (36) Walter, M.; Akola, J.; Lopez-Acevedo, O.; Jadzinsky, P. D.; Calero, G.; Ackerson, C. J.; Whetten, R. L.; Grönbeck, H.; Häkkinen, H. A Unified View of Ligand-Protected Gold Clusters as Superatom Complexes. *Proc. Natl. Acad. Sci. U. S. A.* **2008**, *105*, 9157–9162.